

Lattice dynamics effects on the magnetocrystalline anisotropy energy: application to MnBi

Andrea Urru¹ and Andrea Dal Corso^{1,2}

¹*International School for Advanced Studies (SISSA),
Via Bonomea 265, 34136 Trieste (Italy).*

²*DEMOCRITOS IOM-CNR Trieste (Italy).*

(Dated: September 2, 2020)

Using a first-principles fully relativistic scheme based on ultrasoft pseudopotentials and density functional perturbation theory, we study the magnetocrystalline anisotropy free energy of the ferromagnetic binary compound MnBi. We find that differences in the phonon dispersions due to the different orientations of the magnetization (in-plane and perpendicular to the plane) give a difference between the vibrational free energies of the high-temperature and low-temperature phases. This vibrational contribution to the magnetocrystalline anisotropy energy (MAE) constant, K_u , is non-negligible. When the energy contribution to the MAE is calculated by the PBEsol exchange and correlation functional, the addition of the phonon contribution allows to get a $T = 0$ K K_u and a spin-reorientation transition temperature in reasonable agreement with experiments.

I. INTRODUCTION

Recently, there has been a significant effort toward the realization of rare-earth-free permanent magnets^{1,2}. Due to its magnetic properties, such as a high Curie temperature, well above room temperature, and a large uniaxial magnetic anisotropy, MnBi²⁻⁵ has emerged as a promising candidate among the transition-metal-based materials.

Below the Curie temperature, estimated to be $T_c = 680$ K^{6,7}, MnBi is a ferromagnet which crystallizes in the NiAs structure. Its magnetocrystalline anisotropy energy (MAE) as a function of temperature is peculiar: at $T = 0$ K the MAE constant K_u is negative, its reported experimental value being -0.2 MJ / m³ (≈ -0.12 meV / cell) with an easy axis in the basal plane⁸, and increasing with T , unlike most magnetic systems^{4,8}. At $T \approx 90$ K K_u becomes positive, thus leading to a spin-reorientation transition: from 90 K to 140 K, the easy axis rotates outside the basal plane, and above 140 K it is parallel to the c axis⁹.

Several studies, both experimental and theoretical, have been carried out during the past years to understand this intriguing property. Experiments studied several properties of MnBi, including the thermal expansion. In particular, the spin-reorientation transition comes together with a small kink in the lattice parameters at $T \approx 90$ K^{10,11}, which has been interpreted as the sign of a phase transition. Theoretical calculations, based on Density Functional Theory (DFT) within the Local Density Approximation (LDA) and the Generalized Gradient Approximation (GGA) for the exchange-correlation functional, correctly predict MnBi to be a metal and a ferromagnet in the low-temperature phase, and to have a negative K_u , in agreement with experiments. Yet, they are believed to overestimate the magnitude of K_u by nearly an order of magnitude and are often not able to reproduce the correct behavior of K_u as a function of temperature. Refs. 12 and 13 showed that the treatment of

correlation effects by means of the DFT+U approach is important to get the correct behavior of K_u as a function of temperature. In particular, in Ref. 13 the inclusion of the thermal expansion effects on K_u allowed to get a spin-reorientation temperature in agreement with experiments and a theoretical MAE in good agreement with experimental results, especially in the temperature range 150-450 K.

More recently, in Ref. 14 it was suggested that the spin-reorientation phenomenon might be partially due to lattice dynamics. Such statement was supported by the calculation of the lattice dynamics contribution to K_u , obtained by averaging the MAE over configurations in which the Mn and Bi atoms were displaced according to the mean square atomic displacements as a function of temperature.

Recently, we extended Density Functional Perturbation Theory (DFPT) for lattice dynamics with Fully Relativistic (FR) Ultrasoft pseudopotentials (US-PPs) to magnetic materials¹⁵. The new formulation allows to detect differences in the phonon frequencies for different orientations of the magnetization, thus making possible to evaluate the vibrational free energy contribution to the MAE.

In this paper we study, by means of ab-initio techniques, the lattice dynamics of ferromagnetic MnBi for two different orientations of the magnetization: 1. in-plane; 2. perpendicular to the plane. We find that the two phonon dispersions mainly differ in the high-frequency optical branches, where the phase with magnetic moments pointing in the out-of-plane direction shows, on average, phonon modes of 2 cm⁻¹ lower in frequency. Starting from the difference of the vibrational density of states of the two phases we compute the vibrational contribution to MAE. We find that, if the energy contribution to MAE is computed by the PBEsol exchange-correlation functional, the phonon contribution is of the same order of magnitude as the ground state MAE, hence it plays a relevant role in the calculation of K_u and to

determine the spin-reorientation transition temperature T_{SR} .

II. METHODS

First-principle calculations were carried out by means of DFT^{16,17} within the LDA¹⁸ and the Perdew-Burke-Ernzerhof optimized for solids (PBEsol)¹⁹ schemes for the exchange-correlation functional approximation, as implemented in the Quantum ESPRESSO^{20–22} and thermo_pw²³ packages. The atoms are described by FR US-PPs²⁴, with $3p$, $4s$, and $3d$ electrons for Mn (PPs `Mn.rel-pz-spn-rrkjus_psl.0.3.1.UPF` and `Mn.rel-pbesol-spn-rrkjus_psl.0.3.1.UPF`, from `pslibrary 0.3.1`^{25,26}) and with $6s$, $5d$, and $6p$ electrons for Bi (PPs `Bi.rel-pz-dn-rrkjus_psl.1.0.0.UPF` and `Bi.rel-pbesol-dn-rrkjus_psl.1.0.0.UPF`, from `pslibrary 1.0.0`^{25,26}).

MnBi crystallizes in the NiAs structure, with an hexagonal lattice described by the point group D_{6h} . The inclusion of magnetism differentiates the structures into a low-symmetry phase ($\mathbf{m} \perp \mathbf{c}$ henceforth), below T_{SR} , and a high-symmetry phase ($\mathbf{m} \parallel \mathbf{c}$ henceforth), above T_{SR} . In particular, the $\mathbf{m} \parallel \mathbf{c}$ phase is described by the magnetic point group $D_{6h}(C_{6h})$, compatible with an hexagonal Bravais lattice, while the $\mathbf{m} \perp \mathbf{c}$ phase has a magnetic point group $D_{2h}(C_{2h})$, compatible with a base-centered orthorhombic Bravais lattice. We checked the relevance of the lattice parameter b , which is not constrained by symmetry in the $\mathbf{m} \perp \mathbf{c}$ phase, and concluded that it is not crucial to make the structure more stable than the $\mathbf{m} \parallel \mathbf{c}$ phase, hence in the rest of the paper we use the ideal value $b = \sqrt{3}a$. In Table I we summarize the data relative to the lattice constants and to the magnetic moment of Mn atoms, obtained with the LDA and PBEsol functionals, and compare them with previous theoretical results and with experiments. The LDA geometry is in good agreement with the theoretical results reported in Ref. 14, but both lattice constants underestimate the experimental values: in particular, a is 2 % smaller than experiment, while c is 8 % smaller than experiment. The PBEsol geometry gives lattice constants slightly smaller than PBE (reported in Ref. 14) and experiments: a and c are 0.5 % and 6 % smaller than experiment, respectively. The $\mathbf{m} \perp \mathbf{c}$ and $\mathbf{m} \parallel \mathbf{c}$ phases have slightly different lattice constants a and c , but in Table I we report only one structure because the differences in the lattice constants are beyond the significative digits reported. In this paper we use the LDA to compute the phonon frequencies and their contribution to the MAE, while the PBEsol is used to compute the energy contribution to the MAE and to correct it for thermal expansion effects. The LDA and the PBEsol (at $T = 0$ K) calculations are performed at the geometry reported in Table I. The computed Mn magnetic moment m_{Mn} is in agreement with previous calculations reported in literature^{12,14}: m_{Mn} is 10 % (20 %) smaller than experiment within the PBEsol (LDA)

Exchange-correlation functional	a (Å)	c (Å)	m_{Mn} (μ_B)
LDA (this work)	4.16	5.57	3.2
LDA (Ref. 14)	4.20	5.54	3.29
GGA-PBEsol (this work)	4.24	5.67	3.5
GGA-PBEsol (Ref. 14)	4.28	5.63	3.56
GGA-PBE (Ref. 14)	4.35	5.76	3.69
GGA-PBE (Ref. 12)	4.31	5.74	3.45
GGA-PBE + U (Ref. 12)	4.39	6.12	3.96
exp. (Ref. 10)	4.27	6.05	3.8-4.2

Table I. Computed (FR LDA and PBEsol), theoretical reference (LDA, PBEsol, PBE, and PBE+U), and experimental lattice constants and Mn magnetic moments.

approximation.

The pseudo wave functions (charge density) have been expanded in a plane waves basis set with a kinetic energy cut-off of 110 (440) Ry. The Brillouin Zone (BZ) integrations have been done using a shifted uniform Monkhorst-Pack mesh²⁷ of $12 \times 12 \times 8$ \mathbf{k} -points. The presence of a Fermi surface has been dealt with by the Methfessel-Paxton smearing method²⁸, with a smearing parameter $\sigma = 0.015$ Ry. The dynamical matrices have been computed on a uniform $4 \times 4 \times 3$ \mathbf{q} -points mesh, and a Fourier interpolation was used to obtain the complete phonon dispersions and the free energy. The latter has been obtained approximating the BZ integral with a $300 \times 300 \times 300$ \mathbf{q} -points mesh.

III. RESULTS

MnBi is a magnetic binary compound, in which magnetism is carried mainly by the Mn atoms, while Bi is responsible for a strong spin-orbit interaction. As a consequence, strong magnetocrystalline anisotropy effects are expected.

Phonon dispersions

Here we consider the phonon dispersions of MnBi with two different orientations of the magnetic moments, $\mathbf{m} \perp \mathbf{c}$ (in-plane) and $\mathbf{m} \parallel \mathbf{c}$ (out-of-plane), and among all the possible in-plane orientations $\mathbf{m} \perp \mathbf{c}$, we choose $\mathbf{m} \parallel \mathbf{a}$, \mathbf{a} and \mathbf{c} being the primitive vectors of the hexagonal Bravais lattice). The presence of a magnetization leads to a difference in the Bravais lattice the magnetic point group is compatible with, as discussed in the previous Section. In order to compare the phonon dispersions in the same BZ, we choose to set the geometry in the base-centered orthorhombic Bravais lattice, which is compatible with the low-symmetry phase (magnetic point group $D_{2h}(C_{2h})$).

The phonon dispersions are illustrated in Fig. 1. The phonon modes are split in two groups, separated by a

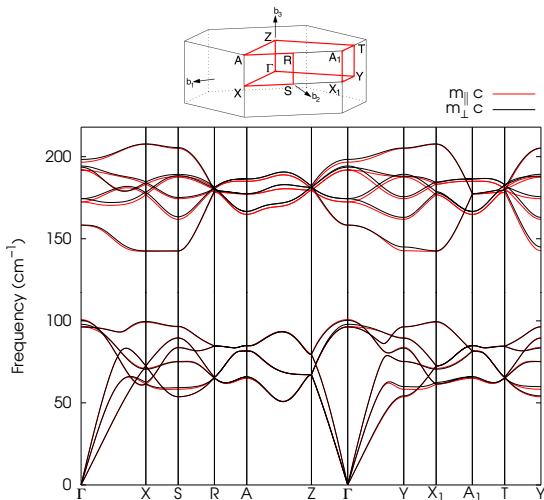


Figure 1. Computed FR LDA phonon dispersions of MnBi with magnetic moments oriented in plane ($\mathbf{m} \perp \mathbf{c}$, black line), and out of plane ($\mathbf{m} \parallel \mathbf{c}$, red line).

gap. The low-frequency branches (up to $\sim 100 \text{ cm}^{-1}$) are dominated by displacements of the heavy element Bi, while the high-frequency branches (from $\sim 150 \text{ cm}^{-1}$ to $\sim 200 \text{ cm}^{-1}$) are mainly displacements of the Mn atoms. The main difference between the phonon frequencies of the two phases is a rigid shift: the phonon frequencies of the phase with in-plane magnetization are higher than those of the phase with out-of-plane magnetization. The shift is about 0.5 cm^{-1} in the low-frequency branches, while it is about 2 cm^{-1} in the high-frequency branches. Moreover, there are differences due to symmetry. The system with in-plane magnetization has lower symmetry and some modes, degenerate when the magnetization is along \mathbf{c} , split. As an example, in Table II we report the phonon modes at Z and X_1 . At Z, in the phase with $\mathbf{m} \parallel \mathbf{c}$ there are two groups of four-fold degenerate modes, which become four couples of degenerate modes in the phase $\mathbf{m} \perp \mathbf{c}$: the splittings are quite small, in the range $0.02\text{-}0.08 \text{ cm}^{-1}$. At X_1 , in the configuration $\mathbf{m} \parallel \mathbf{c}$ there are four two-fold degenerate modes, which split from 0.1 cm^{-1} to 1 cm^{-1} . Similar splittings are found also along the other high-symmetry lines.

MAE

In previous works, the spin-reorientation transition, due to the change of K_u from negative to positive at $T_{SR} \approx 90 \text{ K}$, has been explained as an effect of thermal expansion of the crystal parameters a and c .

In Refs. 12 and 13 $K_u^{th.exp.}$, the function K_u obtained accounting for thermal expansion effects, has been computed within the LSDA + SO (spin-orbit) + U scheme using the experimental lattice constants as a function of the temperature, reported in Refs. 10 and 11 and finding in this way a good agreement with experiments.

q	$\mathbf{m} \parallel \mathbf{c}$		$\mathbf{m} \perp \mathbf{c}$	
	$\nu \text{ (cm}^{-1}\text{)}$	degeneracy	$\nu \text{ (cm}^{-1}\text{)}$	degeneracy
Z	67.135	4	67.212	2
	180.245	4	181.263	2
X_1	61.427	2	61.554	1
	72.461	2	62.503	1
			72.467	1
			72.577	1
	176.735	2	178.156	1
			178.556	1
		185.195	1	
		185.395	1	

Table II. Computed FR LDA phonon frequencies at high-symmetry points Z and X_1 for the configurations $\mathbf{m} \parallel \mathbf{c}$ and $\mathbf{m} \perp \mathbf{c}$. Only the degenerate modes are shown for the configuration $\mathbf{m} \parallel \mathbf{c}$, and how the degeneracy is lowered or lifted if $\mathbf{m} \perp \mathbf{c}$.

Here instead we compute $K_u^{th.exp.}$ within the FR PBEsol scheme. In Fig. 2(a) we show \bar{K}_u , the contribution to K_u given by the energy difference of the electronic ground-states, for a mesh of geometries and on top of it we indicate with black and white points the thermal expansion data added to the theoretical PBEsol $T = 0 \text{ K}$ crystal parameters. The resulting $K_u^{th.exp.}$ is reported in Fig. 2(b). $K_u^{th.exp.}$ is negative and slightly increases with increasing a and c . Yet, such an increase is not sufficient to cross the value $K_u^{th.exp.} = 0$ because the $T = 0 \text{ K}$ energy difference ($\approx -0.73 \text{ meV/cell}$) is significantly lower than the experimental value ($\approx -0.15 \text{ meV/cell}$), similarly to what found within the LDA and GGA approximations in Refs. 12 and 13, and because the energy difference landscape shows a local maximum of about -0.4 meV/cell .

In addition to the thermal expansion effect we consider also the effect of the lattice dynamics on K_u : in fact, since the two phases have slightly different phonon frequencies, they have different vibrational entropies that give a temperature-dependent contribution to the MAE defined as the difference of the vibrational free energies of the two phases. We write the constant K_u as²⁹:

$$K_u = K_u^{th.exp.} + K_u^{vib} + K_u^{mag}, \quad (1)$$

where $K_u^{th.exp.}$ is the thermal expansion contribution, K_u^{vib} is the lattice dynamics contribution, and K_u^{mag} is the magnon contribution, which we do not consider in the present work. The term K_u^{vib} can be computed from the phonon frequencies using the harmonic approximation:

$$K_u^{vib} = \int_0^{+\infty} d\omega \frac{1}{2} \hbar \omega [g_{\perp}(\omega) - g_{\parallel}(\omega)] + k_B T \int_0^{+\infty} d\omega [g_{\perp}(\omega) - g_{\parallel}(\omega)] \ln \left(1 - e^{-\hbar \omega / k_B T} \right), \quad (2)$$

where $g_{\perp}(\omega)$ ($g_{\parallel}(\omega)$) is the phonon density of states relative to the phase with $\mathbf{m} \perp \mathbf{c}$ ($\mathbf{m} \parallel \mathbf{c}$). In our case K_u^{vib}

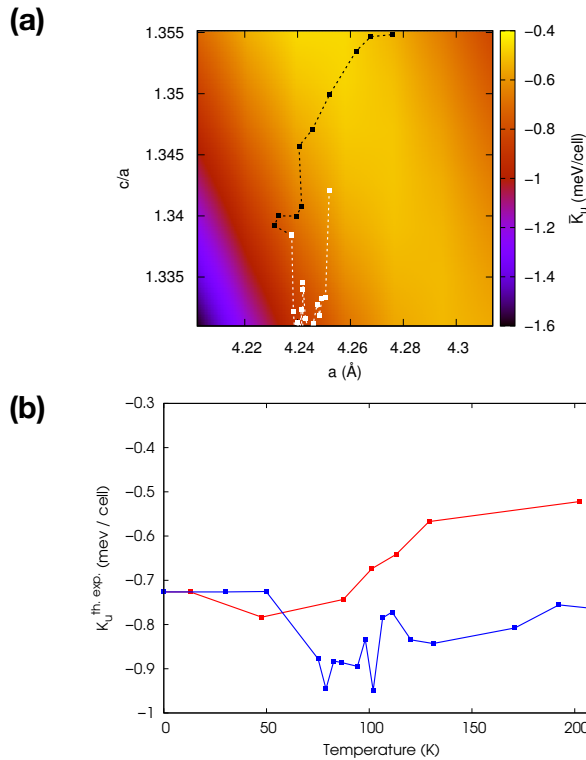


Figure 2. Energy contribution to the MAE constant, \bar{K}_u , computed in the FR PBEsol scheme. (a) \bar{K}_u as a function of lattice constants. Black and white dashed lines represent the geometries at different temperatures, obtained from Refs. 10 and 11, respectively, as explained in the main text. (b) $K_u^{th.exp}$ as a function of temperature. Red and blue lines represent the values of $K_u^{th.exp}$ obtained from the black and white dashed lines of Fig. 2 (a), respectively.

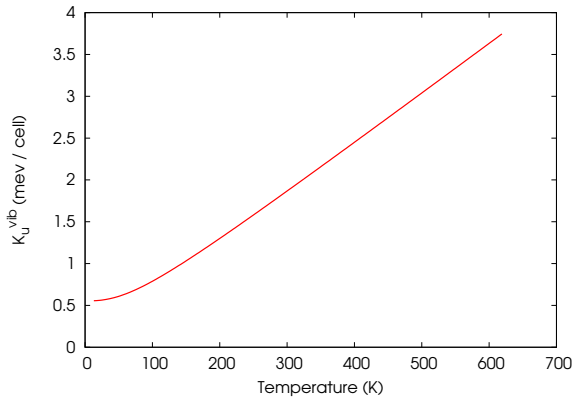


Figure 3. Vibrational contribution to the MAE constant K_u , computed from the phonon frequencies within the harmonic approximation (Eq. (2))

is always positive and increases with increasing temperature, as shown in Fig. 3: its magnitude is comparable

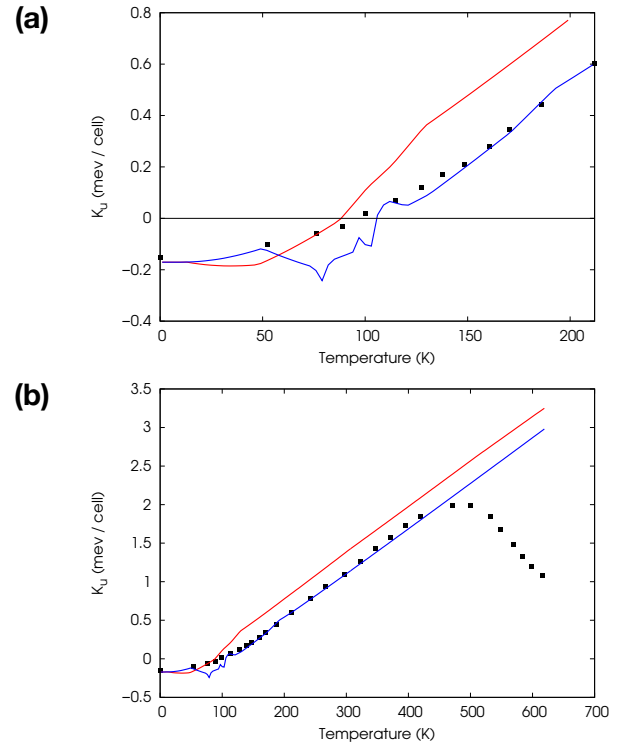


Figure 4. Comparison between computed and experimental MAE constant K_u . Black squares represent experimental data⁸, red and blue lines represent the total K_u computed, where the $K_u^{th.exp}$ contribution has been obtained from Refs. 10 and 11, respectively, as explained in the main text. (a) Detailed comparison in the temperature range 0 – 200 K, to highlight T_{SR} . (b) Comparison in a wider range of temperatures (0 – 600 K).

with that of $K_u^{th.exp}$, hence it gives a crucial contribution in determining the MAE constant K_u .

In Figs. 4(a-b) we show the total K_u defined in Eq. (1) and compare it with the experimental data. By comparison with Fig. 2(b), it is clear that the addition of the vibrational contribution is important. In particular, the zero-point vibrational free energy difference allows to have a $T = 0$ K value of K_u in good agreement with experiments and, together with the thermal contribution (second term of Eq. (2)), to get a transition temperature T_{SR} in reasonable agreement with the experiments ($T_{SR} \approx 90$ K and $T_{SR} \approx 110$ K with the data given by Refs. 10 and 11, respectively). Moreover, the vibrational contribution allows to have a fair agreement with experimental data⁸ in a rather large temperature range, as shown in Fig. 4(b). At variance with Ref. 13, we do not find a maximum in K_u because the $T = 0$ K geometry corresponds to the theoretical geometry and because the vibrational contribution increases with T . At high temperatures ($T > 500$ K) our results do not agree with the experiment, suggesting that additional contributions may become important in this temperature range, in particular the term K_u^{mag} in Eq. (1), which can result in a

decreasing K_u with T^{30} . Moreover, we mention that in the high-temperature limit additional effects not included in Eq. (1), as the magnon-phonon coupling^{31,32}, might be non-negligible.

IV. CONCLUSIONS

By means of recent developments in first-principles theoretical tools, we have studied the lattice dynamics of the MnBi ferromagnet for two orientations of the magnetization, $\mathbf{m} \perp \mathbf{c}$ and $\mathbf{m} \parallel \mathbf{c}$. We have shown that the differences in the phonon frequencies give rise to a contribution to the MAE that is comparable with the electronic one. We have found that the vibrational contribution is relevant to explain the behavior of the MAE constant K_u as a function of temperature. We could also get an estimate of the spin-reorientation temperature T_{SR} in fair agreement with the experimental value using the PBEsol approximation to evaluate the energy contribution to the MAE. The use of other functionals such as LDA would give instead a lower value of the MAE

at $T = 0$ K than that predicted by PBEsol, and would lead to predict $T_{SR} \approx 500$ K. The use of the Hubbard U parameter would result, instead, in a higher value of K_u at $T = 0$ K¹³ and, as a consequence, we would get $K_u > 0$ when adding the vibrational contribution, thus the spin-reorientation transition would not be explained.

In Ref. 14 a first estimate of the vibrational contribution to MAE was given, which led to $T_{SR} \approx 450$ K, far from the experimental value. In this work we have found a vibrational contribution of the same order of magnitude as found in Ref. 14, and we have included also the zero-point vibrational free energy difference, which gives an important contribution and leads to an estimated spin-reorientation temperature $T_{SR} \approx 100$ K, when used together with the energy MAE given by PBEsol.

ACKNOWLEDGMENTS

Computational facilities have been provided by SISSA through its Linux Cluster and ITCS and by CINECA through the SISSA-CINECA 2019-2020 Agreement.

-
- ¹ D. J. Sellmyer, B. Balamurugan, W. Y. Zhang, B. Das, R. Skomski, P. Kharel, and Y. Liu, *Advances in Rare-Earth-Free Permanent Magnets*. In: Marquis F. (eds) *Proceedings of the 8th Pacific Rim International Congress on Advanced Materials and Processing*. Springer, Cham; DOI: https://doi.org/10.1007/978-3-319-48764-9_212 (2013).
- ² J. Cui, M. Kramer, L. Zhou, F. Liu, A. Gabay, G. Hadjipanayis, B. Balasubramanian, D. Sellmyer, *Acta Materialia* **158**, 118-137; DOI: <https://doi.org/10.1016/j.actamat.2018.07.049> (2018).
- ³ C. Guillaud, *J. Phys. Radium* **12**, 143; DOI: [10.1051/jphysrad:01951001202014300](https://doi.org/10.1051/jphysrad:01951001202014300) (1951).
- ⁴ B. W. Roberts, *Phys. Rev.* **104**, 607; DOI: [10.1103/PhysRev.104.607](https://doi.org/10.1103/PhysRev.104.607) (1956).
- ⁵ J. B. Yang, K. Kamaraju, W. B. Yelon, and W. J. James, *Appl. Phys. Lett.* **79**, 1846; DOI: [10.1063/1.1405434](https://doi.org/10.1063/1.1405434) (2001).
- ⁶ T. Chen, *J. Appl. Phys.* **45**, 2358; DOI: [10.1063/1.1663594](https://doi.org/10.1063/1.1663594) (1974).
- ⁷ M. A. McGuire, H. Cao, B. C. Chakoumakos, and B. C. Sales, *Phys. Rev. B* **90**, 174425; DOI: <https://doi.org/10.1103/PhysRevB.90.174425> (2014).
- ⁸ W. E. Stutius, T. Chen, and T. R. Sandin, *Magnetism and magnetic materials - 1973: Nineteenth Annual Conference*, DOI: [10.1063/1.2947245](https://doi.org/10.1063/1.2947245) (1974).
- ⁹ T. Hihara and Y. Kōi, *J. Phys. Soc. Jpn.* **29**, 343; DOI: <https://doi.org/10.1143/JPSJ.29.343> (1970).
- ¹⁰ J. B. Yang, Y. B. Yang, X. G. Chen, X. B. Ma, J. Z. Han, Y. C. Yang, S. Guo, A. R. Yan, Q. Z. Huang, M. M. Wu et al., *Appl. Phys. Lett.* **99**, 082505; DOI: <https://doi.org/10.1063/1.3630001> (2011).
- ¹¹ K. Koyama, Y. Mitsui, and K. Watanabe, *Sci. Technol. Adv. Mater.* **9**, 024204; DOI: <https://doi.org/10.1088/1468-6996/9/2/024204> (2008).
- ¹² N. A. Zarkevich, L.L. Wang, and D. D. Johnson, *APL Mater.* **2**, 032103; DOI: <https://doi.org/10.1063/1.4867223> (2014).
- ¹³ V. P. Antropov, V. N. Antonov, L. V. Bekenov, A. Kutepov, and G. Kotliar, *Phys. Rev. B* **90** 054404; DOI: [10.1103/PhysRevB.90.054404](https://doi.org/10.1103/PhysRevB.90.054404) (2014).
- ¹⁴ K. V. Shanavas, D. Parker, and D. J. Singh, *Sci. Reports* **4**, 7222; DOI: [10.1038/srep07222](https://doi.org/10.1038/srep07222) (2014).
- ¹⁵ A. Urru and A. Dal Corso, *Phys. Rev. B* **100**, 045115; DOI: <https://doi.org/10.1103/PhysRevB.100.045115> (2019).
- ¹⁶ P. Hohenberg and W. Kohn, *Phys. Rev.* **136**, B864; DOI: <https://doi.org/10.1103/PhysRev.136.B864> (1964).
- ¹⁷ W. Kohn and L. J. Sham, *Phys. Rev.* **140**, A1133; DOI: <https://doi.org/10.1103/PhysRev.140.A1133> (1965).
- ¹⁸ J. P. Perdew and A. Zunger, *Phys. Rev. B* **23**, 5048; DOI: <https://doi.org/10.1103/PhysRevB.23.5048> (1981).
- ¹⁹ J. P. Perdew, A. Ruzsinszky, G. I. Csonka, O. A. Vydrov, G. E. Scuseria, L. A. Constantin, X. Zhou, and K. Burke, *Phys. Rev. Lett.* **100**, 136406; DOI: <https://doi.org/10.1103/PhysRevLett.100.136406> (2008).
- ²⁰ P. Giannozzi, S. Baroni, N. Bonini, M. Calandra, R. Car, C. Cavazzoni, D. Ceresoli, G. L. Chiarotti, M. Cococcioni, I. Dabo, et al., *J. Phys. Condens. Matter* **21**, 395502; DOI: [10.1088/0953-8984/21/39/395502](https://doi.org/10.1088/0953-8984/21/39/395502) (2009) (See <http://www.quantum-espresso.org>).
- ²¹ P. Giannozzi, O. Andreussi, T. Brumme, O. Bunau, M. B. Nardelli, M. Calandra, R. Car, C. Cavazzoni, D. Ceresoli, M. Cococcioni, et al., *J. Phys. Condens. Matter* **29**, 465901; DOI: doi.org/10.1088/1361-648X/aa8f79 (2017).
- ²² P. Giannozzi, O. Baseggio, P. Bonfá, D. Brunato, R. Car, I. Carnimeo, C. Cavazzoni, S. de Gironcoli, P. Delugas, F. Ferrari Ruffino, et al., *J. Chem. Phys.* **152**, 154105; DOI: <https://doi.org/10.1063/5.0005082> (2020).
- ²³ `thermo_pw` is an extension of the `Quantum ESPRESSO (QE)` package which provides an alternative organization of the

- QE work-flow for the most common tasks. For more information see https://dalcorso.github.io/thermo_pw.
- ²⁴ A. Dal Corso and A. Mosca Conte, Phys. Rev. B **71**, 115106; DOI: <https://doi.org/10.1103/PhysRevB.71.115106> (2005).
- ²⁵ A. Dal Corso, Comp. Mat. Sci. **95**, 337; DOI: <https://doi.org/10.1016/j.commatsci.2014.07.043> (2014).
- ²⁶ See <https://dalcorso.github.io/pslibrary>.
- ²⁷ H. J. Monkhorst and J.D. Pack, Phys. Rev. B **13**, 5188; DOI: <https://doi.org/10.1103/PhysRevB.13.5188> (1976).
- ²⁸ M. Methfessel and A.T. Paxton, Phys. Rev. B **40**, 3616; DOI: <https://doi.org/10.1103/PhysRevB.40.3616> (1989).
- ²⁹ F. Körmann, A. Dick, B. Grabowski, B. Hallstedt, T. Hickel, and J. Neugebauer, Phys. Rev. B **78**, 033102; DOI: <https://doi.org/10.1103/PhysRevB.78.033102> (2008).
- ³⁰ J. B. Staunton, S. Ostanin, S. S. A. Razee, B. L. Gyorffy, L. Szunyogh, B. Ginatempo, and E. Bruno, Phys. Rev. Lett. **93**, 257204; DOI: <https://doi.org/10.1103/PhysRevLett.93.257204> (2004).
- ³¹ F. Körmann, A. Dick, B. Grabowski, T. Hickel, and J. Neugebauer, Phys. Rev. B **85**, 125104; DOI: <https://doi.org/10.1103/PhysRevB.85.125104> (2012).
- ³² J. Hellsvik, D. Thonig, K. Modin, D. Iusan, A. Bergman, O. Eriksson, L. Bergqvist, and A. Delin, Phys. Rev. B **99**, 104302; DOI: <https://doi.org/10.1103/PhysRevB.99.104302> (2019).